applied sciences

MDPI

Article

Precipitation and Calcination of High-Capacity $LiNiO_2$ Cathode Material for Lithium-Ion Batteries

Juho Välikangas [1,*], Petteri Laine [1], Marianna Hietaniemi [1], Tao Hu [1], Pekka Tynjälä [1,2] and Ulla Lassi [1]

1 Research Unit of Sustainable Chemistry, University of Oulu, P.O. Box 4000, FI-90014 Oulu, Finland; petteri.laine@chydenius.fi (P.L.); marianna.hietaniemi@chydenius.fi (M.H.); tao.hu@oulu.fi (T.H.); pekka.tynjala@chydenius.fi (P.T.); ulla.lassi@oulu.fi (U.L.)

2 University of Jyvaskyla, Kokkola University Consortium Chydenius, Talonpojankatu 2B, FI-67100 Kokkola, Finland

* Correspondence: juho.valikangas@oulu.fi; Tel.: +358-50-350-7699

Received: 30 November 2020; Accepted: 15 December 2020; Published: 16 December 2020

Abstract: This article presents the electrochemical results that can be achieved for pure $LiNiO_2$ cathode material prepared with a simple, low-cost, and efficient process. The results clarify the roles of the process parameters, precipitation temperature, and lithiation temperature in the performance of high-quality $LiNiO_2$ cathode material. $Ni(OH)_2$ with a spherical morphology was precipitated at different temperatures and mixed with LiOH to synthesize the $LiNiO_2$ cathode material. The $LiNiO_2$ calcination temperature was optimized to achieve a high initial discharge capacity of 231.7 mAh/g (0.1 C/2.6 V) with a first cycle efficiency of 91.3% and retaining a capacity of 135 mAh/g after 400 cycles. These are among the best results reported so far for pure $LiNiO_2$ cathode material.

Keywords: lithium-ion battery; LNO; cathode; lithium nickel oxide

1. Introduction

$LiCoO_2$, introduced by J. B. Goodenough [1], was the first layered transition metal oxide used in commercial Li-ion batteries and has since become the most common cathode material for rechargeable batteries [2]. However, cobalt is very expensive and has been subsequently replaced partially by other metals to decrease the manufacturing costs of the cathode materials [3]. A common type of mixed metal oxide, NCM333, was first introduced by Ohzuku et al. [4] in 2001 and has an equal mix of nickel, cobalt, and manganese. Cathode materials with a high nickel content ($LiNi_xCo_yMe_1$-x-yO_2. $x \geq 0.8$–1.0) have attracted much interest as lithium storage materials for rechargeable lithium batteries. These layered oxide materials typically have high energy densities (>200 mAh/g) but suffer from low thermal stability and capacity fading during cycling. Recently, the focus has been on high nickel-containing, mixed-metal oxides, tailored especially for the demand of electric vehicles [3,5].

Pure $LiNiO_2$ is an interesting candidate for cathode material in Li-ion batteries, because most of its high theoretical capacity of 274 mAh/g is utilizable at a reasonable voltage range between 2.6 and 4.2 V and the material is low cost. For these reasons, it has been under study for over 15 years [6–8]. However, the electrochemical and structural stability results noted by earlier studies lacked promise, driving interest towards $LiCoO_2$ and mixed $LiNi_xCo_yMn_zO_2$ materials [9]. Recent published articles about the synthesis conditions of $LiNiO_2$ include Bianchini et al.'s [10] structural study, which showed a low lithiation temperature of 650–700 °C would annihilate most defects in the $LiNiO_2$'s crystal structure. Deng et al. [11] went further, showing that an electrolyte dopant can stabilize $LiNiO_2$ cells.

The present study focuses on the development of a continuous and simple process for producing high quality $LiNiO_2$. This work will provide direction for future work on preparing and testing different dopants, coatings, and other subjects relating to the performance of $LiNiO_2$ cathode material.

2. Materials and Methods

2.1. Precipitation of $Ni(OH)_2$ Precursors

Spherical $Ni(OH)_2$ precursors were synthetized by using hydroxide co-precipitation under an inert atmosphere, according to the literature [12,13]. Precipitation was carried out in a continuous flow reactor with a volume of three liters at temperatures of 40, 50, or 60 °C under vigorous mixing at 1150 rpm. The reactor was preloaded with deionized water; then, aqueous solutions of 1 M $NiSO_4 \cdot 6H_2O$, 2.5 mol/L NaOH, and concentrated ammonia were fed separately to the reactor using peristaltic pumps. The feeding rates of the reactants were optimized in order to achieve a residence time of 4 h as well as the desired precipitation pH level and ammonia concentration in the reactor.

Particle growth during precipitation was analyzed by determining the particle size distribution of the slurry sampled from the overflow tubing of the reactor. After a precipitation time of 12 h, the precursor slurry was filtered under reduced pressure, and the precipitate was washed carefully with a sufficient amount of deionized water. The synthetized $Ni(OH)_2$ precursor was then dried in a vacuum oven at 60 °C overnight.

2.2. Lithiation

The $Ni(OH)_2$ precursor precipitated at 40 °C was mixed with LiOH using a Li:Ni molar ratio of 1.04:1. The LiOH excess was used to compensate for the lithium lost during high-temperature calcination and to ensure homogeneous lithiation. The mixtures were calcined with a 2.5 °C/min heating ramp and a 5 h holding time at different temperatures (650, 670, or 690 °C) in an oxygen atmosphere; samples were later named LN650, LN670, and LN690, according to their respective calcination temperature. The material was subsequently milled and sieved to less than 40 µm in dry room conditions. For the pouch cell tests, the residual lithium was washed from the surface of the secondary particles with deionized water.

2.3. Cell Assembling and Electrochemical Characterization

Electrochemical performance testing was carried out using both half-cells, with metallic lithium as the counter electrode, and full cells, with graphite as the anode material. All electrode foils and battery cells were prepared in dry room conditions.

A cathode slurry was mixed using a mixer (Thinky ARE-250). The slurry composition was 4% polyvinylidene fluoride (Kureha #1100), 4% carbon (Timcal C45), and 92% active material, with 1-methyl-2-pyrrolidinone (Alfa Aesar, anhydrous 99.5%) as a solvent. The slurry was spread on aluminum foil with 100 µm applicators before being dried on a hot plate at 50 °C for a one hour and finally being placed in a vacuum oven at 120 °C overnight.

The cathode foil was calendared three times before coin cell assembly. The active material loading on the foil was about 12 mg/cm^2. Two 2016-type coin cells were assembled from each sample foil with metallic lithium as the counter electrode and 1M LiPF6 in 1:1:1 EC:DEC:DMC as the electrolyte. Cells were cycled 62 times at 25 °C (see Table 1 for the C-rate used). Cells were at first charged at a constant current until 4.3 V was reached, and after that with a constant voltage until the current decreased to 0.015 C for the first two cycles. In subsequent charge cycles, the same method was used but the current threshold was raised to 0.02 C. Discharge for the first two cycles was done at constant current of 0.1 C until 2.6 V was reached and after that with constant voltage until the current decreased to 0.015 C. A subsequent discharge was done to 3.0 V with a constant current. Cells were tested at 25 °C. The theoretical capacity used to calculate the C-rate was 200 mAh/g. One electrode pair pouch cell (50 mAh) was prepared with a graphite anode (Hitachi), an electrolyte of 1.15 M $LIPF_6$ in

EC:DMC:EMC (2:4:4), and 1% vinylene carbonate. After the formation cycles, the pouch cells were at first charged at a constant current 0.5 C until 4.2 V was reached, and after that with a constant voltage until the current decreased to 0.03 C and discharged to 2.5 V at 0.5 C. Every 200 cycles, a capacity check cycle at 0.2 C was run and before the capacity check, the cells were discharged at 0.2 C.

Table 1. Coin cell testing program.

Cycle Number	1	2	3	4	5	6	7–30	31	32–59	61	62
Charge C-rate	0.1 + 0.015	0.1 + 0.015	0.1 + 0.02	0.1 + 0.02	0.1 + 0.02	0.1 + 0.02	0.2 + 0.02	0.2 + 0.02	0.2 + 0.02	0.2 + 0.02	0.1 + 0.02
Discharge C-rate	0.1 + 0.015	0.1 + 0.015	0.2	0.33	0.5	1	2	0.2	2	0.2	0.1
Voltage range	4.3 V–2.6 V	4.3 V–2.6 V	4.3 V–3.0 V	4.3 V–3.0 V	4.3 V–3.0 V	4.3 V–3.0 V	4.3 V–3.0 V	4.3 V–3.0 V	4.3 V–3.0 V	4.3 V–3.0 V	4.3 V–3.0 V

2.4. Characterization of Samples

The tapped density of the powders was measured using an Erweka SVM222 tapped density device and following the ISO EN 787/11 standard. Residual lithium was measured with an automatic titrator. Particle size distribution (PSD) during precipitation was measured with a Malvern Mastersizer 3000.

X-ray diffraction (XRD) was measured with Rigaku SmartLab 9 kW X-ray diffractometers and using Co as a source at 40 kV, 135 mA. Diffractograms were collected in the 2θ range (5–120° at 0.01° intervals) with a scan speed of 4.06 deg/min. Peaks were identified using the database of the International Centre for Diffraction Data (PDF-4 + 2020). The crystallite sizes as well as anisotropy and distribution were computed using the Rikagu PDXL2 analysis package. The Whole Powder Pattern Fitting (WPPF) was used with the decomposition and least square Pawley method. The peak shape was modelled using the FP (Fundamental Parameter) method with continuous scan and the Cheary–Coelho Axial model, using experimental geometry and optics. The crystallite shape was refined as an ellipsoidal shape, with a lognormal distribution used as the free parameter for iterative refinement other than spherical shape, which is a better fit for the crystal structure of $LiNiO_2$. The site occupancy was analyzed using the Rietveld model by PDXL2.

The microstructures shown in the field-emission scanning electron microscopy (FESEM) images was obtained using a Zeiss Sigma FESEM operating at 5 kV. Both XRD and FESEM were performed at the Centre for Material Analysis of the University of Oulu.

3. Results and Discussion

3.1. Effect of Precipitation on Crystal Growth

The morphology of the precipitated $Ni(OH)_2$ particles was followed and is presented in Figure 1. According to the FESEM imaging, the higher precipitation temperature created more closely packed primary particles and started cracking the secondary particles. The particle morphology shown in Figure 1 is comparable to that reported by Yang et al. [12]. During the reaction-crystallization precipitation process in an aqueous solution, the $Ni(OH)_2$ particles are known to evolve from an amorphous state to spherical particles with sizes ranging from nanometers to several microns. According to the proposed mechanism, growth on crystallite templates in the radial direction is free and fast, but the growth rate in other directions is restricted due to a short supply of monomers. As only radially arranged crystallites grow quickly, the resulting macrospherical $Ni(OH)_2$ particles were characterized by large radially arranged platelet-like crystallites [14].

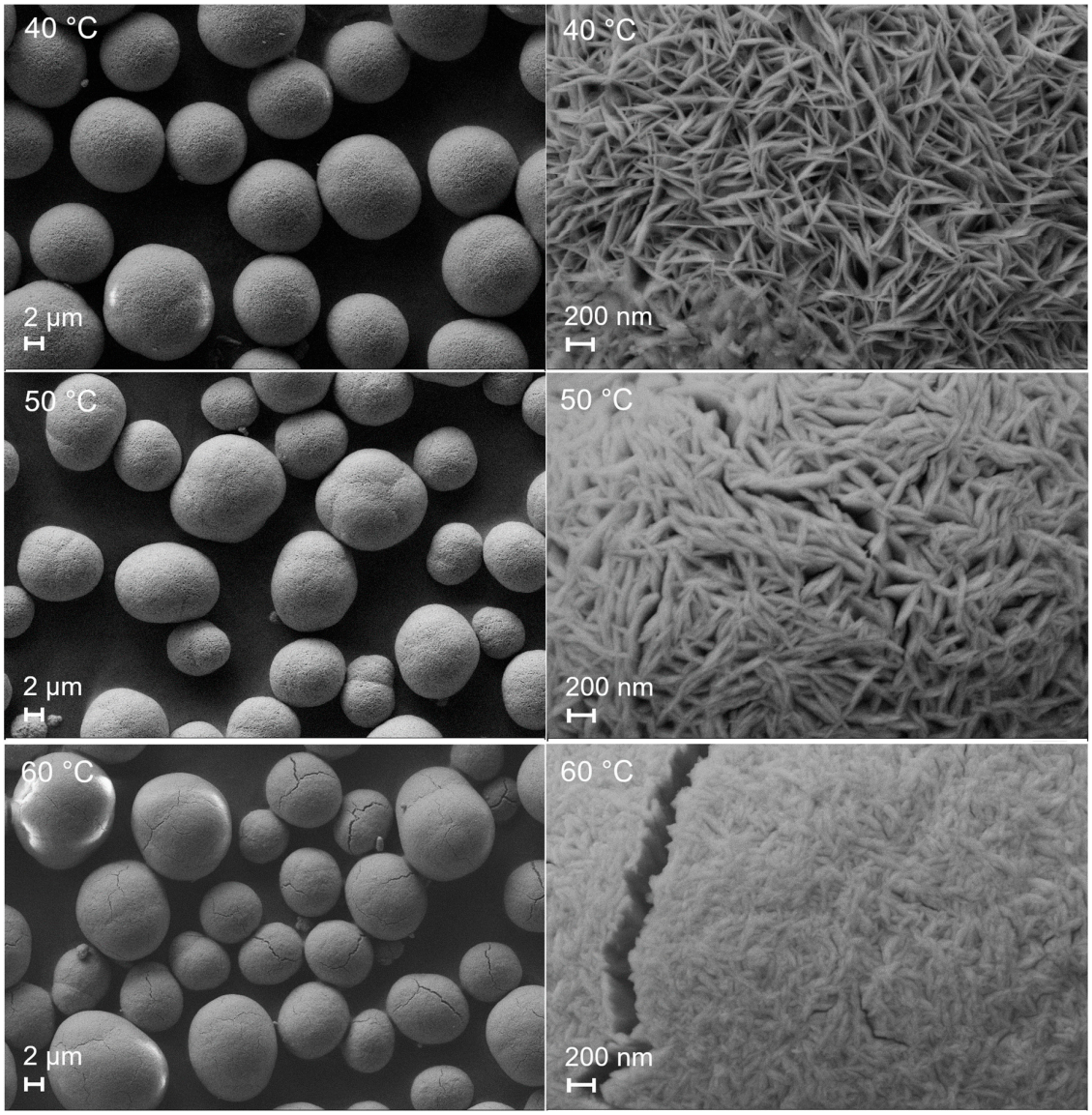

Figure 1. SEM images of the $Ni(OH)_2$ particles precipitated at 40, 50, or 60 °C. Magnitudes are 5000× and 75,000×.

The PSD is correspondingly visible in Figure 2, with the measured PSD curves after precipitation times of 6, 8, 10, and 12 h as well as after a maturation period of 12 h. Table 2 shows the tap densities of the samples prepared at different precipitation temperatures, illustrating that higher temperatures created a higher tap density. The precursor precipitated at 40 °C was subsequently lithiated at different temperatures, indicating a good tap density for $LiNiO_2$ after the lithiation process (Table 2).

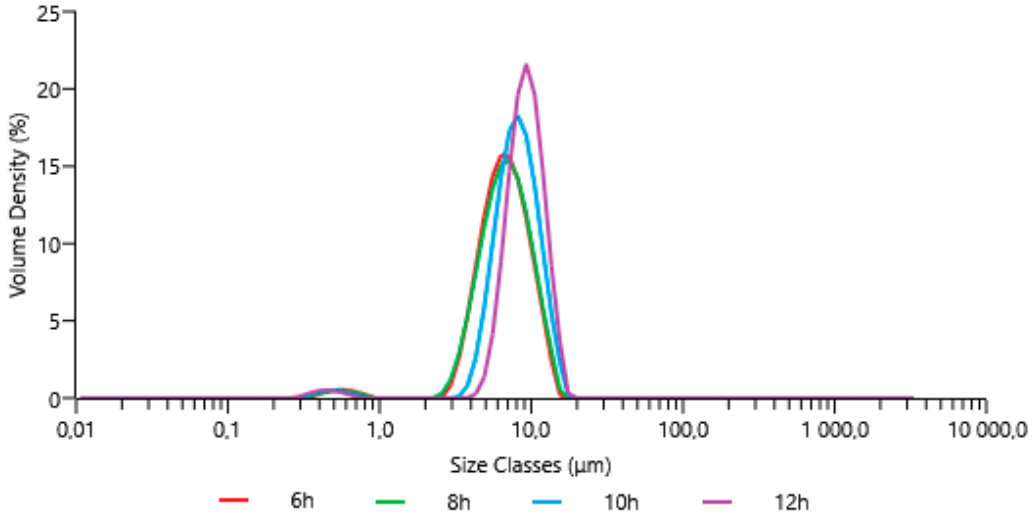

Figure 2. Particle size distribution (PSD) curves after precipitation times of 6, 8, 10, and 12 h.

Table 2. Tap density results for the $Ni(OH)_2$ precursors lithiated at 670 °C.

Sample	T.de (g/mL) $Ni(OH)_2$	T.de (g/mL) $LiNiO_2$
Ni12 (40 °C)	1.86	2.56
Ni14 (50 °C)	2.00	
Ni15 (60 °C)	2.07	

3.2. XRD Results and Discussion

Table 3 shows the XRD lattice parameters that agree with the previously published values for stoichiometric $LiNiO_2$ [6,7,15]. Specifically, Dahn et al. [15] showed XRD lattice parameter values for different $Li_{1\pm x}NiO_2$ compositions that agree well with our values for stoichiometric $LiNiO_2$. LN670 presented the highest c/3a value, indicating samples with the lowest cation–anion mixing in a structure [2]. Despite this, the values for the different samples were notably close to each other. The crystallite size increases with the temperature, as can be expected.

Table 3. XRD parameters for the samples.

Sample	C-Axis (Å)	A-Axis (Å)	C/a	c/3a Ratio	(003)/(104) Integrated Ratio	Crystallite Size a (Å)	Crystallite Size c (Å)
LN650	14.1919(2) [1]	2.87638(2) [1]	4.9339	1.64465	1.306	1579.6(9) [1]	1973(1) [1]
LN670	14.1929(1) [1]	2.87646(1) [1]	4.9342	1.64471	1.338	2419.9(9) [1]	3773(1) [1]
LN690	14.1989(1) [1]	2.87882(1) [1]	4.9322	1.64406	1.294	2854.8(9) [1]	4119(1) [1]

[1] The error of the crystallite sizes 14.1919(2) means 14.1919 ± 0.0002, 1579.6(9) means 1579.6 ± 0.9.

Ohzuku et al. (1993) showed that electroactive $LiNiO_2$ showed larger integrated intensity ratios of I(003)/I(104) and a clear split of the (108) and (110) peaks [7]. LN670 showed the highest integrated intensity ratios of I(003)/I(104) and highest discharge capacity (see Table 4). Figure 3 shows the $LiNiO_2$ structure without impurity phases and magnifications of the split peaks (108) and (110). The LN650 split of the (108) and (110) peaks is not as clear as that of the LN670 and LN690 samples.

Table 4. First cycle performance and capacity retention after 62 cycles.

Sample	Charge 4.3 V 0.1 C + 0.015 C (1st)	DC 3.0 V 0.1 C (1st)	DC 2.6 V 0.1 C (1st)	0.1 C Eff 3.0 v (1st)	0.1 C Eff. 2.6 v (1st)	DC 3.0 V 0.1 C (62)	Retention After 62 Cycles
	mAh/g	mAh/g	mAh/g	%	%	mAh/g	%
LN650	250.9	218.4	223.1	87.0	89.0	193.3	88.5
LN670	253.8	227.2	231.7	89.5	91.3	188.0	82.8
LN690	252.0	221.9	225.6	88.1	89.5	165.5	74.6

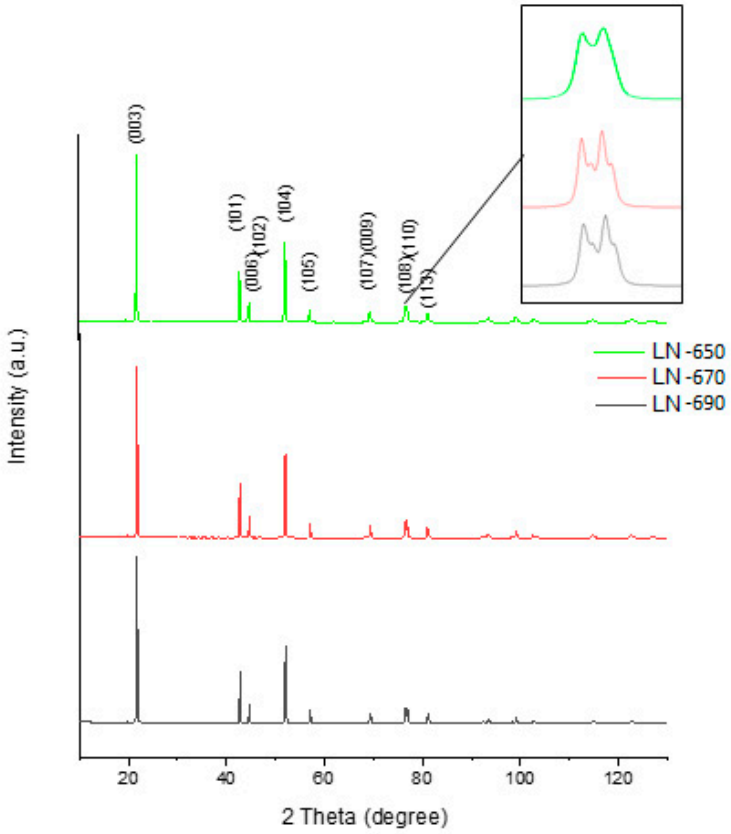

Figure 3. XRD pattern for the prepared $LiNiO_2$ materials.

Table 5 shows the lattice occupancies of the Li, Ni, and O sites determined by Rietveld refinement. The refinement was done by Rietveld refinement, the FP (Fundamental Parameter peak shape) method with continuous scan, and the Cheary–Coelho Axial model, using experimental geometry and optics. Constraints on total occupancy of Wyckoff sites 3a and 3b being equal to 1 (Ni + Li = 1). The ESD was the standard deviation from the refinement process, which means the estimated error from the iterative, least squares method computation. From the Ni1(3b) value, which is the ratio of lithium sites occupied by nickel, it showed that LN670 has the lowest amount of cation mixing (occupancy of 0.0128), which actually supports 670 °C being the best lithiation temperature. Zhang et al. [16] claimed that under 2% of cation mixing does not affect the electrochemical performance of the $LiNi_{0.33}Mn_{0.33}Co_{0.33}O_2$ (NMC111) cathode material.

Table 5. Lattice occupancies of the Li, Ni, and O sites.

		LN670	LN670 (ESD)	LN690	LN690 (ESD)	LN650	LN650 (ESD)
Li1 (3a)	x	0		0		0	
	y	0		0		0	
	z	0		0		0	
	Occ.	0.0114	0.0017	0.0029	0.0017	0.0095	0.0020
Ni1(3b)	x	0		0		0	
	y	0		0		0	
	z	0.5		0.5		0.5	
	Occ.	0.0128	0.0005	0.0248	0.0005	0.0166	0.0007
Ni2(3a)	x	0		0		0	
	y	0		0		0	
	z	0		0		0	
	Occ.	0.9886	0.0017	0.9971	0.0017	0.9905	0.0020
Li2(3b)	x	0		0		0	
	y	0		0		0	
	z	0.5		0.5		0.5	
	Occ.	0.9872	0.0005	0.9752	0.0005	0.9834	0.0007
O1	x	0		0		0	
	y	0		0		0	
	z	0.258		0.258		0.257724	
	Occ.	1.0000	0.0000	1.0000	0.0000	1.0000	0.0000
	Rwp (%)	6.26		6.13		5.26	

3.3. SEM Images of $LiNiO_2$

The FESEM images in Figure 4 show that the $LiNiO_2$ secondary particles retained their round-shaped morphology during the mixing, lithiation, milling, and sieving processes. The images in Figure 4, shown at 75,000× magnification, illustrate the secondary particle surfaces and how the primary particle size increases with lithiation temperature.

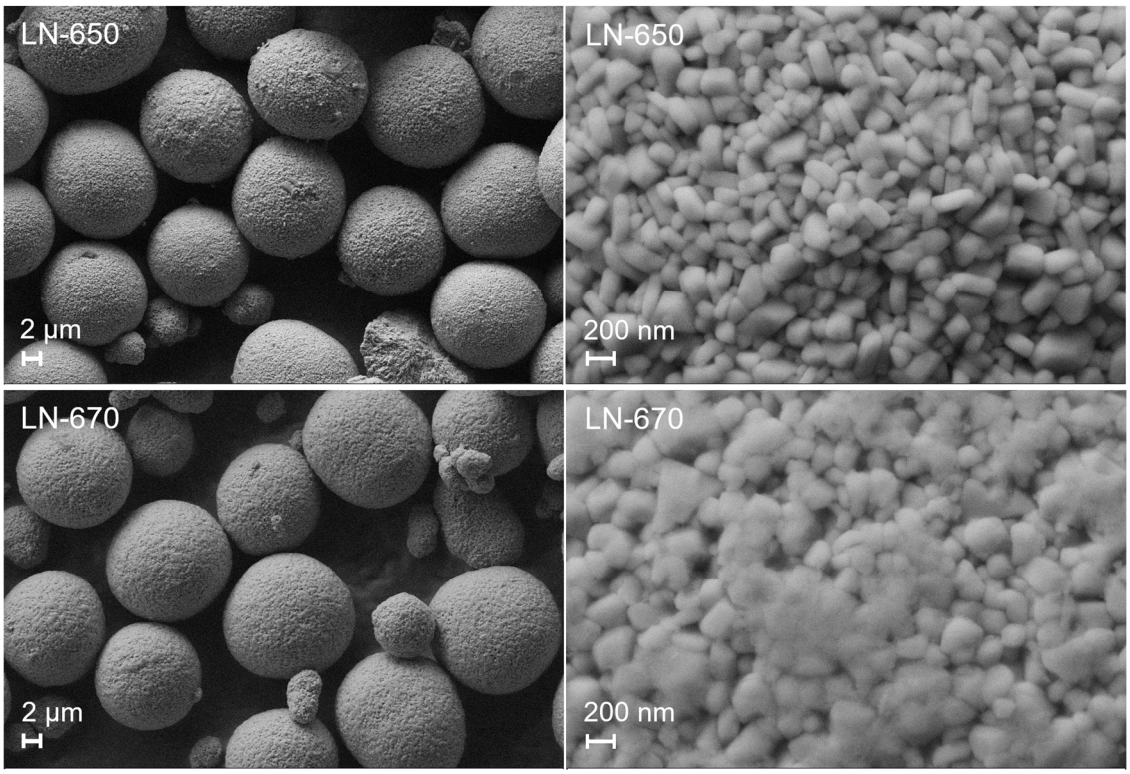

Figure 4. *Cont.*

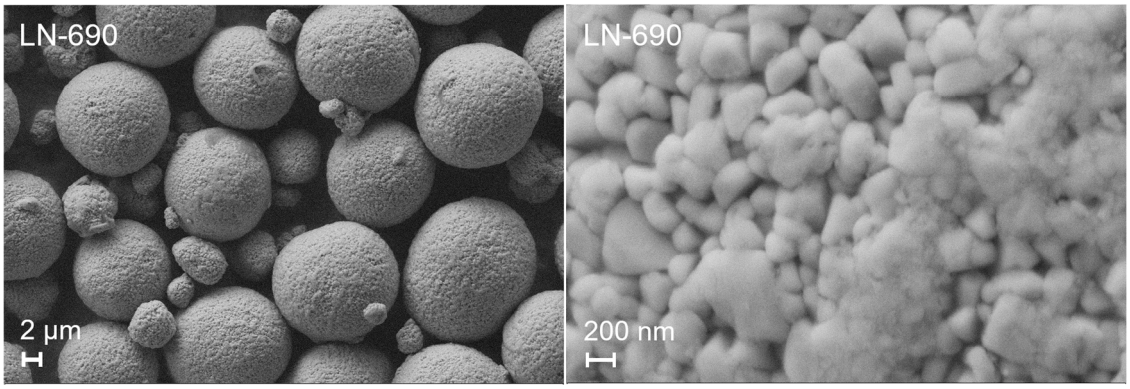

Figure 4. SEM images of LN650, LN670, and LN690 at magnitudes of 5000× and 75,000×.

3.4. Electrochemical Performance

Table 4 shows the first cycle performance and capacity retention after the testing program. LN670 had the highest first cycle efficiency (91.3%) and discharge capacity (231 mAh/g), one of the highest ever reported for $LiNiO_2$. [17–19]. Higher and lower lithiation temperatures produced lower capacities and lower efficiency, but the lowest lithiation temperature also showed improved capacity retention.

In Table 6, the discharge capacity results from previously published research articles are presented for comparison. As can be seen in Table 6, results of Yoon et al. [17] show the highest first cycle capacity of 246.6 mAh/g. There are, however, some differences in the electrochemical testing conditions between our work and the work of Yoon et al. For example, lower current and higher testing temperatures used in the article of Yoon et al. can increase the first cycle capacity.

Table 6. The first cycle discharge capacities and testing conditions from reference articles.

	Testing Conditions			
Result (mAh/g)	**Current (mA/g)**	**Voltage Range (V)**	**T (°C)**	**Ref.**
231.7	20	4.3–2.6	25	This article
246.6	18	4.3–2.7	30	[16]
220.2	22.5	4.3–3.0	25	[18]
199	21	4.27–2.6		[17]

Table 7 shows the rate performance of the $LiNiO_2$ materials. Cells were charged at 0.1 C to 4.3 V and at a constant voltage until 0.02 C was reached. Cells were subsequently discharged at different rates (0.2 C, 0.33 C, 0.5 C, 1 C, and 2 C). Results indicate the best results were produced by the LN670 sample regardless of the discharge rate.

Table 7. Rate performances of the tested samples.

	Charge 0.1 C + 0.02 C –>4.3 V–>DC 3.0 V				
Sample	**DC 0.2 C mAh/g**	**DC 0.33 C mAh/g**	**DC 0.5 C mAh/g**	**DC 1 C mAh/g**	**DC 2 C mAh/g**
LN650	215.5	210.2	206.0	201.3	195.3
LN670	217.4	211.6	207.1	202.9	196.5
LN690	208.3	201.7	197.0	191.8	185.6

Figure 5a shows the first cycle charge and discharge voltage curves for the different LNO samples. Figure 5b shows the discharge voltage curves at different C rates for sample LN670. Up to 0.5 C voltage, the plateaus are clearly different, but at 1 C and 2 C, the plateaus start fading. Figure 5c shows the charge and discharge curves for cells charged to different cut-off voltages. Cut-off voltages of 4.3 V

and 4.2 V show similar voltage plateaus, but cells with 4.15 V and 4.1 V the highest voltage plateau vanish. Figure 5d shows the cyclability curves for cells with different cut-off voltages, indicating that the 4.3 V and 4.2 V cut-off voltages possess a similar capacity and capacity retention, while 4.15 V and 4.1 V bear a lower capacity but excellent capacity retention. Yoon et al. [17] presented similar results, claiming that a better capacity retention was due to a lower level of particle cracking for cells with lower voltage cut-offs.

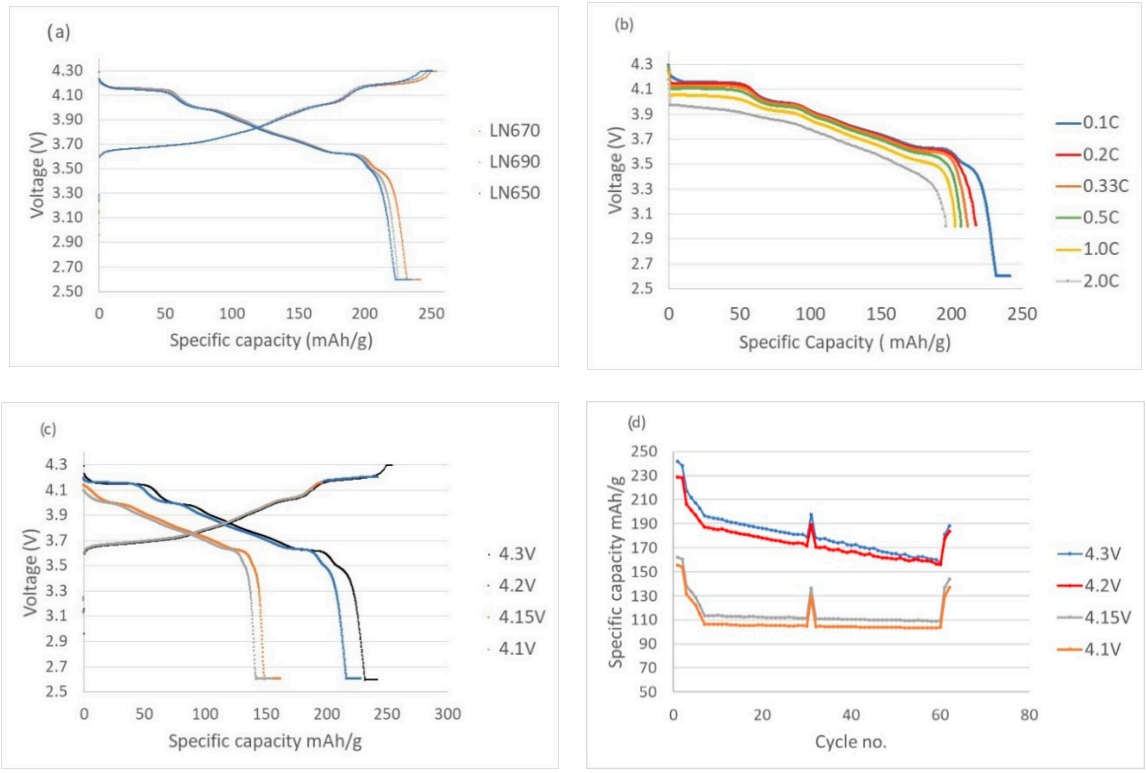

Figure 5. (**a**) First cycle charge and discharge curves for different samples. (**b**) Discharge curves at different rates (0.1, 0.2, 0.33, 0.5, 1, and 2 C) from the LN670 sample. (**c**) First cycle charge and discharge curves for cells from the LN670 sample with different cut-off voltages. (**d**) Cycling curves for the cells with different cut-off voltages from the LN670 sample.

Table 8 shows the excess lithium before (LN670) and after the washing procedure (LN670-W). Results showed that washing effectively reduced the lithium from the particle surfaces.

Table 8. Li/Me ratio measured by ICP-OES and residual lithium measured with automatic titration.

Sample	ICP Li/Me	Residual Li Li_2CO_3 (wt.%)	LiOH (wt.%)	Li (wt.%)
LN-670	1.08	0.92	1.38	0.57
LN670-W	1.01	0.19	0.19	0.09

Figure 6 shows pouch cell discharge capacity retention during the cycles. The unwashed sample capacity was higher at the beginning but decreased quickly. A high amount of residual lithium on the unwashed particle surfaces can react with electrolytes and produce gases, causing bad contacts in the cell [18,20,21]. The washing procedure can remove lithium from the $LiNiO_2$ structure, which might explain the lower capacity at the beginning of the tests [18]. The capacity remaining for the washed sample after 400 cycles was 135 mAh/g at 0.2 C.

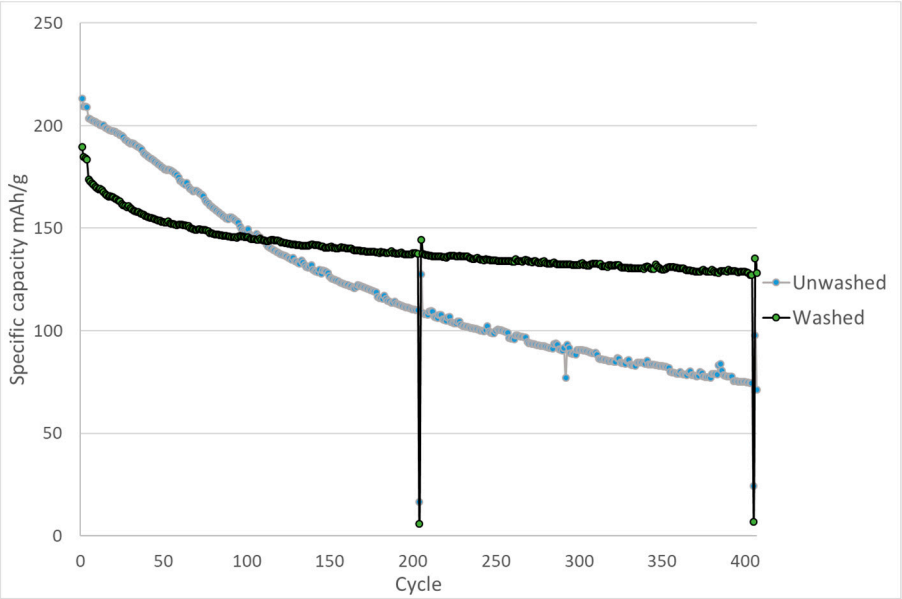

Figure 6. Pouch cell testing results for washed and unwashed LN670 samples.

4. Conclusions

$Ni(OH)_2$ precipitation was performed by applying different temperatures, with the results showing that it is possible to change the precursor particle morphology and tap density by changing the precipitation temperature within a range of 40–60 °C.

The lithiated $LiNiO_2$ samples showed good properties according to electrochemical studies. The optimal lithiation temperature to achieve high capacity and good capacity retention was found to be 670 °C. Lower cut-off voltages resulted in better capacity retention during coin cell testing, and the results were similar to those of previous studies. Pouch cell results showed that residual lithium compounds on particle surfaces are critical for the cycling properties, and that washing procedures should be optimized to avoid the delithiation of the $LiNiO_2$ structure. Future work will focus on different elemental doping during precipitation and coating during the lithiation process. Different cut-off voltages will be tested in pouch cells to see how they stabilize cells for long-term cycling tests.

Author Contributions: Conceptualization: J.V., P.L., P.T., M.H., T.H. and U.L.; methodology: J.V., P.L., P.T., M.H., T.H.; validation: J.V., P.L., P.T., M.H., T.H.; formal, analysis: J.V., T.H.; investigation: J.V., T.H.; resources: J.V., P.L., T.H., M.H., P.T.; data curation: J.V., P.L., P.T., M.H., T.H.; writing—original draft preparation: J.V., P.L., P.T., M.H., T.H. and U.L.; writing—review and editing: J.V., P.L., P.T., M.H., T.H. and U.L.; visualization: J.V., P.L., P.T., M.H., T.H. and U.L.; supervision: U.L.; project administration: U.L.; funding acquisition: U.L. All authors have read and agreed to the published version of the manuscript.

Funding: This research was funded by Business Finland, grant number (University of Oulu, BATCircle, Dnro 5877/31/2018).

Acknowledgments: M.Sc. Marcin Selent, Centre for Material Analysis, University of Oulu, is acknowledged for the help with XRD analysis.

Conflicts of Interest: The authors declare no conflict of interest.

References

1. Mizushima, K.; Jones, P.C.; Wiseman, P.J.; Goodenough, J.B. $LixCoO_2$ ($0 < x < -1$): A new cathode material for batteries of high energy density. *Mater. Res. Bull.* **1980**, *15*, 783–789. [CrossRef]
2. Whittingham, M.S. Lithium Batteries and Cathode Materials. *Chem. Rev.* **2004**, *104*, 4271–4302. [CrossRef] [PubMed]

3. Kim, Y.; Seong, W.M.; Manthiram, A. Cobalt-free, high-nickel layered oxide cathodes for lithium-ion batteries: Progress, challenges, and perspectives. *Energy Storage Mater.* **2021**, *34*, 250–259. [CrossRef]
4. Ohzuku, T.; Makimura, Y. Layered Lithium Insertion Material of LiCo1/3Ni1/3Mn1/3O_2 for Lithium-Ion Batteries. *Chem. Lett.* **2001**, *30*, 642–643. [CrossRef]
5. Manthiram, A.; Song, B.; Li, W. A perspective on nickel-rich layered oxide cathodes for lithium-ion batteries. *Energy Storage Mater.* **2017**, *6*, 125–139. [CrossRef]
6. Arai, H. Characterization and cathode performance of $Li_{1-x}Ni_{1+x}O_2$ prepared with the excess lithium method. *Solid State Ion.* **1995**, *80*, 261–269. [CrossRef]
7. Ohzuku, T.; Ueda, A.; Nagayama, M. Electrochemistry and Structural Chemistry of $LiNiO_2$ (R3m) for 4 Volt Secondary Lithium Cells. *J. Electrochem. Soc.* **1993**, *140*, 1862–1870. [CrossRef]
8. Megahed, S.; Ebner, W. Lithium-ion battery for electronic applications. *J. Power Sources* **1995**, *54*, 155–162. [CrossRef]
9. Hirano, A. Relationship between non-stoichiometry and physical properties in $LiNiO_2$. *Solid State Ion.* **1995**, *78*, 123–131. [CrossRef]
10. Bianchini, M.; Fauth, F.; Hartmann, P.; Brezesinski, T.; Janek, J. An in situ structural study on the synthesis and decomposition of $LiNiO_2$. *J. Mater. Chem. A Mater. Energy Sustain.* **2020**, *8*, 1808–1820. [CrossRef]
11. Deng, T.; Fan, X.; Cao, L.; Chen, J.; Hou, S.; Ji, X.; Chen, L.; Li, S.; Zhou, X.; Hu, E.; et al. Designing In-Situ-Formed Interphases Enables Highly Reversible Cobalt-Free LiNiO2 Cathode for Li-ion and Li-metal Batteries. *Joule* **2019**, *3*, 2550–2564. [CrossRef]
12. Yang, C. Synthesis and characterization of active materials of Ni(OH) 2 powders. *Int. J. Hydrog. Energy* **2002**, *27*, 1071–1081. [CrossRef]
13. Weiwei, E.; Cheng, J.; Yang, C.; Mao, Z. Experimental study by online measurement of the precipitation of nickel hydroxide: Effects of operating conditions. *Chin. J. Chem. Eng.* **2015**, *23*, 860–867. [CrossRef]
14. Peng, M.-X.; Shen, X.-Q. Template Growth Mechanism of Spherical $Ni(OH)_2$. *J. Cent. South Univ. Technol.* **2007**, *14*, 310–314. [CrossRef]
15. Dahn, J. Structure and electrochemistry of Li1±yNiO_2 and a new Li_2NiO_2 phase with the Ni $(OH)_2$ structure. *Solid State Ion.* **1990**, *44*, 87–97. [CrossRef]
16. Zhang, X.; Jiang, W.J.; Mauger, A.; Qilu; Gendron, F.; Julien, C.M. Minimization of the cation mixing in $Li_{1+x}(NMC)_{1-x}O_2$ as cathode material. *J. Power Sources* **2010**, *195*, 1292–1301. [CrossRef]
17. Yoon, C.S.; Jun, D.; Myung, S.; Sun, Y. Structural Stability of $LiNiO_2$ Cycled above 4.2 V. *ACS Energy Lett.* **2017**, *2*, 1150–1155. [CrossRef]
18. Moshtev, R.; Zlatilova, P.; Vasilev, S.; Bakalova, I.; Kozawa, A. Synthesis, XRD characterization and electrochemical performance of overlithiated $LiNiO_2$. *J. Power Sources* **1999**, *81–82*, 434–441. [CrossRef]
19. De Biasi, L.; Schiele, A.; Roca-Ayats, M.; Garcia, G.; Brezesinski, T.; Hartmann, P.; Janek, J. Phase Transformation Behavior and Stability of $LiNiO_2$ Cathode Material for Li-Ion Batteries Obtained from InSitu Gas Analysis and Operando X-Ray Diffraction. *ChemSusChem* **2019**, *12*, 2240–2250. [CrossRef]
20. Imhof, R. Oxidative Electrolyte Solvent Degradation in Lithium-Ion Batteries: An In Situ Differential Electrochemical Mass Spectrometry Investigation. *J. Electrochem. Soc.* **1999**, *146*, 1702–1706. [CrossRef]
21. Renfrew, S.E.; McCloskey, B.D. Residual Lithium Carbonate Predominantly Accounts for First Cycle CO_2 and CO Outgassing of Li-Stoichiometric and Li-Rich Layered Transition-Metal Oxides. *J. Am. Chem. Soc.* **2017**, *139*, 17853–17860. [CrossRef] [PubMed]